Biomaterials Science

In Situ Preparation of Gold-Polyester Nanoparticles for Biomedical Imaging

Journal:	*Biomaterials Science*
Manuscript ID	BM-ART-02-2020-000175.R1
Article Type:	Paper
Date Submitted by the Author:	30-Mar-2020
Complete List of Authors:	Attia, Mohamed; Clemson University, Chemistry Ranasinghe, Meenakshi ; Clemson University, Chemistry Akasov, Roman; Russian Academy of Sciences Anker, Jeffrey; Clemson University, Chemistry Whitehead, Daniel; Clemson University, Department of Chemistry Alexis, Frank; University Yachay Tech, School of Biological Science and Engineering

In Situ Preparation of Gold-Polyester Nanoparticles for Biomedical Imaging

Mohamed F. Attia,[a] Meenakshi Ranasinghe,[a] Roman Akasov,[c,d] Jeffrey N. Anker, [a] Daniel C. Whitehead, [a] and Frank Alexis[b]**

[a]Department of Chemistry, Clemson University, Clemson, SC, USA
[b]School of Biological Sciences and Engineering, Yachay Tech, San Miguel de Urcuquí, Ecuador
[c]National University of Science and Technology «MISIS», Leninskiy Prospect 4, 119991 Moscow, Russia
[d]I.M. Sechenov First Moscow State Medical University, 119991, Trubetskaya str. 8-2, Moscow, Russia

Corresponding Authors: Frank Alexis (falexis@yachaytech.edu.ec) and Daniel C. Whitehead (dwhiteh@clemson.edu)

Abstract

The synthesis and application of gold nanoparticles (AuNPs) have attracted much attention due to their interesting optical and chemical properties, as well as their utility in imaging, therapeutics, sensors, electronics, and catalysis. AuNPs are synthesized using multiple approaches, followed by chemical modification or encapsulation, to enhance their colloidal stability, biocompatibility, and targeting. Here, we report the one-step synthesis of gold-polyester nanoparticles for use as an imaging agent. The AuNPs were prepared inside polymeric NPs by means of ultraviolet irradiation of a gold salt in the presence of Irgacure I-2959 photoinitiator. We monitored the kinetic growth and nucleation of AuNPs (*in vitro* and *ex vivo*) over time using spectral analysis. Moreover, we investigated the cytotoxicity, localized plasmonic surface resonance (LSPR), and cellular imaging capabilities of the Au-polyester nanoparticles. The resulting Au-polyester NPs were characterized by Fourier transform infrared spectroscopy (FTIR), thermogravimetric analysis (TGA), X-ray diffraction (XRD), dynamic light scattering (DLS), and transmission electron microscopy

(TEM) to probe their chemical structure, size, zeta potential (ζ), and morphology, respectively. Furthermore, *in vitro* experiments showed that the NP formulation is stable over time and exhibits negligible toxicity against 3T3 fibroblast and U-87 MG glioblastoma cells. The results also demonstrated that the Au-polyester NPs exhibit excellent cellular imaging properties. This one-step strategy goes beyond current syntheses of gold-polyester nanoparticles because it can be used to synthesize the imaging agent *in situ* (*i.e.*, in living cells) in lieu of conventional *ex situ* approaches.

Keywords

Photochemical synthesis; gold nanoparticles; polyester; cellular imaging; PDLLA; bioimaging

1. Introduction

AuNPs have found use in a wide range of applications such as catalysis,[1] electronics,[2,3] solar cells,[4,5] chemical sensing,[6,7] optical imaging,[6,7] and particularly in therapy and bioimaging. Notably, AuNPs alone – or in combination with other nanomaterials – are applied in targeted photothermal ablation *in vivo* and have been extended to potential clinical studies.[8–14] They also possess antitumor activity[15–17] and can be targeted to tumor cells via passive or active targeting strategies.[18–22] As imaging agents, they are mainly used for CT imaging and provide a higher X-ray attenuation relative to traditional, marketed iodinated molecules and other clinical products.[23,24] The use of AuNPs as contrast agents is also recommended for patients who are contraindicated for iodinated agents. There have been numerous approaches explored for tuning the size, morphology, and surface chemistry of AuNPs in order to optimize the performance of the resulting material for a desired application.[25–27] A number of publications have outlined the common approaches for the synthesis of AuNPs. Chemical methods include the citrate reduction method,[28] the one-phase amine-based method,[29,30] and the Brust-Schiffrin method of two-phase synthesis with thiol stabilization.[31] Alternative strategies include sonochemical methods,[32] laser ablation,[33,34] thermolytic processes,[35,36] and photochemical and radical-induced methods.[37–41] The photochemical synthesis of metal nanoparticles provides the possibility of controlling the rate of NP formation[42] as well as allowing for spatial and temporal control. AuNPs have been chemically functionalized on the surface, encapsulated, or coated in order to enhance their stability, biocompatibility, or targeting capability. Two conventional

approaches to prepare gold-polymer nanoparticles are to mix gold nanoparticles with polymers or to functionalize the surface of gold nanoparticles with an appropriate polymer.[43–46] Nonetheless, this approach requires multiple steps and is mostly based on the principles of surface chemistry or self-assembly. Therefore, when the nanoparticle imaging agents are administered, the imaging contrast is evident in multiple tissues where they are accumulated. To address some of these challenges, we hypothesized that a new gold-polyester nanoparticle formulation for imaging applications could be synthesized *in situ* and in one step using a photochemical synthesis protocol.

Thus, in contrast to conventional approaches to prepare gold-polymer nanoparticles, we report a one-step strategy that allows for the *in situ* preparation of AuNPs embedded within PDLLA-PEG polymeric NPs using a photochemical reaction. Our results validate the use of polymeric NPs bearing a gold salt and photoinitiator to prepare AuNPs on demand upon UV irradiation *in vitro* and *ex vivo* and with possible application for *in vivo* synthesis. The AuNP-polymer nanoparticles were fully characterized by Fourier-transform infrared spectroscopy (FTIR), thermogravimetric analysis (TGA), X-ray diffraction (XRD), dynamic light scattering (DLS), and transmission electron microscopy (TEM). The performance of the Au-polyester NPs in localized surface plasmon resonance (LSPR) and cellular imaging applications was also investigated.

2. Experimental section

2.1. Materials

Hydroxyl poly(ethyleneglycol) carboxyl (HO-PEG-COOH, MW 3500 Da) was supplied by JenKem Technology, D,L-lactide (DLLA, PURASORB DL) was supplied by Purac Biomaterials. Tin(II) 2-ethylhexanoate, anhydrous sodium sulfate, anhydrous toluene, methanol, chloroform, dichloromethane, and poly(vinyl alcohol) (MW 31,000-50,000 Da, 98-99% hydrolyzed (PVA)) were supplied by Sigma-Aldrich. Gold(III) chloride hydrate ($HAuCl_4 \cdot xH_2O$), 2-Hydroxy-4′-(2-hydroxyethoxy)-2-methylpropiophenone (Irgacure I-2959, photoinitiator), deionized water, ultra-centrifugal filters of 100,000 MWCO (Millipore, Billerica, MA) were also employed. Photochemical reactions were carried out in a UV lamp chamber using black 96-well plates. In addition, the *in vitro* experimental materials used for cellular experiments included Dulbecco's modified Eagle medium (DMEM), fetal bovine serum (FBS), penicillin, streptomycin, phosphate buffered saline (PBS) from PAN Biotech (Aidenbach Germany), 3-(4,5-dimethylthiazol-2-yl)-2,5-diphenyltetrazolium bromide (MTT), and dimethyl sulfoxide (DMSO) from Sigma-

Aldrich. Human glioblastoma U-87 MG cells, 3T3 fibroblast cells, and RAW 264.7 Macrophages were purchased from the American Type Culture Collection (ATCC). The chiken tissue used for the imaging studies was prepared by cutting thin slices of chicken breast fillets obtained from a local grocery, Ingles Market, Inc (Asheville, NC, USA).

4.2. Experimental methods

[redacted]oluene)-

2.2.1. ^{1}H NMR Analysis of the synthesized poly(D,L-lactide)-poly(ethyleneglycol) (PDLLA-PEG-COOH) copolymer

^{1}H NMR spectra were recorded with a Bruker Top Spin 3.0 operating at 400 MHz using deuterated chloroform ($CDCl_3$) as a solvent. Chemical shifts (δ) are expressed in parts per million (ppm), taking tetramethylsilane (TMS) as internal reference. Coupling constants (*J*) are reported in Hz. The resulting ^{1}H NMR data was consistent with previously reported spectra for PDLLA-PEG-COOH copolymer (Figure S1). PDLLA-PEG-COOH polymer: ^{1}H NMR (400 MHz; $CDCl_3$): δ (ppm): 5.03 (q, J = 6.7 Hz, 1H, C**H**-CH_3), 3.64 (s, 4H, C$\mathbf{H_2}$-C$\mathbf{H_2}$-O), and 1.68 (d, J = 6.7 Hz, 3H, CH-C$\mathbf{H_3}$).

2.2.2. Synthesis of gold NPs imbedded within PDLLA-PEG-COOH polymeric nanoparticles

Au-polyester polymeric NPs were formulated by the double emulsion solvent evaporation method.[47] Typically, 1.6 mL of a 21.4 mmol aqueous stock solution of Irgacure I-2959 was warmed to 60 ˚C for 15 min. Next, 1 mL of a 9.6 mmol aqueous stock solution of $HAuCl_4 \cdot xH_2O$ was then added to the photoinitiator solution and the resulting solution was diluted to a total volume of 5.7 mL with additional water. Thereafter, 0.5 mL of DCM containing 25 mg of PDLLA-PEG-COOH polymer as an organic phase was mixed with the aqueous solution by vortexing for 1 min followed by sonication at 20% amplitude for 15 s using a 20 W ultrasonic processor. Afterwards, 1% w/v PVA solution (1 mL) was added and the mixture was sonicated again under the same conditions. The resulting water-in-oil (W/O) microemulsion was then added dropwise to a 0.3% w/v PVA solution (25 mL) with continuous stirring for 2 h to remove the organic solvent. The PDLLA-PEG-COOH polymeric NPs containing gold salt and photoinitiator were then purified and concentrated to 1 mL by centrifugation through centrifugal filter units to remove free initiator and gold. Alternatively, the NPs could be purified by dialysis while the solution was concentrated under a stream of nitrogen overnight.

Into a black 96-well plate, 200 μL of the PDLLA-PEG-COOH NP solution was added to each well and then irradiated at 254 nm (1 cm distance) in a UV lamp dark chamber for 30 min. During the irradiation, the transparent solution was transformed into a ruby color due to the formation of gold nanoparticles. After irradiation, the samples were protected from light by aluminum foil and characterized by spectrophotometric analysis. The same procedure was applied to develop three nanoformulations; *i)* PDLLA-PEG-COOH polymer alone, *ii)* PDLLA-PEG-COOH polymer containing gold salt, and *iii)* water solution containing gold salt and photoinitiator in absence of the polymer. The results demonstrated that gold NPs loaded within polymer nanoparticle matrix can be synthesized only in the presence of the photoinitiator (*vide infra*).

2.3. Physicochemical characterization of Au-polyester nanoparticles

2.3.1. Fourier transform infrared spectroscopy (FTIR)

Infrared spectra were obtained from freeze-dried samples which were placed directly in a Nicolet Magna 550 spectrometer equipped with a NicPlan FT-IR Microscope. All spectra were collected with a 2 cm^{-1} resolution after 32 continuous scans.

2.3.2. Thermogravimetric analysis (TGA)

Lyophilized samples of PDLLA-PEG-COOH and Au-polyester NPs were subjected to TGA analysis in a TA Instruments Hi-Res TGA 2950 thermogravimetric analyzer from 25 to 600 ˚C at a rate of 20 ˚C min^{-1} under nitrogen flow.

2.3.3. X-ray diffraction (XRD) analysis

X-ray diffraction (XRD) was used to determine the nature of the polymeric NPs using a Rigaku Ultima IV diffractometer with Cu Kα radiation. PDLLA-PEG-COOH polymer NPs (with and without AuNPs) were analyzed on a zero background sample holder. Data were collected between 5˚ and 65˚ 2θ at a scan rate of 1 degree per minute in 0.02 degree intervals.

2.3.4. Transmission electron microscopy (TEM) and high resolution TEM (HRTEM)

The size and shape of the developed nanoparticles were evaluated by TEM microscopy. A drop of the nanoparticle suspension was placed on a carbon grid and kept at room temperature to dry and form a film on the top of the carbon grid. The samples were then evaluated using 7600-TEM and 9500-HRTEM techniques with low excitation voltage (10

and 5 keV, respectively), and a sample detector distance of 10 mm. Due to the inherent contrast properties of the materials, they did not need to be coated with staining agents.

2.3.5. Dynamic light scattering microscopy (DLS)

Particle Size and Zeta Potential (ζ) Measurements

Aqueous dispersions of the polymer and Au-polyester NP samples with different polymer concentrations were diluted 20 times in water at ambient temperature prior to analysis. They were then transferred to disposable cuvettes with a detection angle of 173˚ at room temperature. All size measurements for particles were made with dynamic light scattering (DLS) on a Malvern Zetasizer Nano Series, and hydrodynamic size was represented with Z-average values in nanometers. The ζ-potential measurements were performed in disposable folded capillary cells and electrophoretic mobilities were converted to ζ-potential using the Smoluchowski model with a Henry's function value of 1.50.[48] All determinations were reported as the average of three measurements.

2.3.6. Ultraviolet–visible spectroscopy

A UNICAM HELIOS UV-vis spectrophotometer (Varioskan Flash, Thermo Scientific, USA) was used for recording absorbance and to conduct kinetics measurements. The transmission spectra of the samples were collected with different dilutions of the polymeric NPs and Au-polyester NPs over the wavelength range of 300 nm to 700 nm (1 nm resolution).

2.4. In vitro studies

2.4.1. In vitro stability of the NPs in fetal bovine serum (FBS)

In order to evaluate the stability of the Au-polyester NPs in blood serum as a means to evaluate their potential biocompatibility, the experiment was performed through incubation of 0.1 mL of the prepared NPs (three gold nanoformulations; 25, 100, and 200 mg polymer/mL in each formulation) with 0.9 mL FBS with gentle stirring at 37 ˚C for 24 h. An aliquot of the incubated solutions was then taken separately at interval times and measured by DLS to assign Z-average particle diameter and PDI in order to investigate the NP sizes and their agglomeration or interaction with biomacromolecules of the blood serum.

2.4.2. Cytotoxicity (MTT and MTS assays)

The cytotoxicity of the Au-polyester NPs was evaluated using the MTT method on both 3T3 fibroblast cells (normal cell line model), human glioblastoma U-87 MG cells (cancer cell line model) and adipose stromal cells (ASC). Cells were seeded at 10^4 cells per well into a 96-well cell culture plate in Dulbecco's Modified Eagle Medium (DMEM) supplemented with 10% FBS and 1% antibiotic (penicillin-streptomycin) at 37 ˚C under a controlled atmosphere (5% CO_2 and 80% H_2O) for 24 h. The cell culture medium was then replaced by the same medium containing different concentrations of three NPs (*i.e.* polymeric NPs, Au-polyester NPs, and Au-polyester NPs generated by irradiation through a chicken tissue barrier loaded at either 10, 20, 50, 100, 200, 300, 400, or 500 µg/mL). After incubation for another 24 h, the cells were washed with fresh PBS, followed by addition of fresh DMEM containing MTT (100 µL, 0.5 mg/mL in PBS) to each well, and the plate was incubated for 4 h at 37 ˚C. The obtained formazan crystals were dissolved by adding 100 µL DMSO in each well followed by shaking the well-plate for 10 min. The UV absorbance was measured at 570 nm with a microplate reader (Varioskan Flash, Thermo Scientific, USA). Experiments were carried out in triplicate and expressed as a percentage of viable cells compared to the control group. In the case of the MTS method, different concentrations of NPs were used (390, 781, 1526, and 3125 mg/mL) compared with two controls (see Figure S6 in ESI). Afterwards, UV irradiation was applied for 30 min followed by adding 20 µL MTS reagent for each well and incubated for an additional four hours. The absorbance at 490 nm was then determined.

2.4.3. Cellular imaging studies

Cell culture

Murine macrophages (RAW) and human glioblastoma (U-87 MG) cells were grown in DMEM supplemented with 10% fetal bovine serum, 2 µM L-glutamine, 100 µg/mL streptomycin, and 100 U/mL penicillin at 37 ˚C in a 5% CO_2 humidified atmosphere. The medium was replaced every 3-4 days.

Confocal fluorescence microscopy

Cells (murine macrophages (RAW) and human glioblastoma (U-87 MG)) were seeded in 8-well glass chambers (10^4 cells per well) followed by overnight incubation. Then, 250 µL of appropriate working solutions of Au-polyester NPs (1000 µg/mL and 500 µg/mL) in full DMEM medium were added to the cells and the plate was incubated in the dark in a CO_2

incubator for 1 h and 24 h. After incubation, the cells were washed 3 times with cold PBS and stained with Hoechst 33258 dye (50 μM) for 15 min. Optical images were acquired using a Leica TSP SPE confocal microscope. The visualization was performed as described previously by Kim *et al*.[49] A laser wavelength of 543 nm and a dichroic beam splitter (RT 70/30, Leica) were used to excite the intracellular Au-polyester NPs, the focus of cells was adjusted using the differential inference contrast (DIC) and fluorescent Hoechst 33258 staining as a reference.

2.5. Scattering spectrum

Sample preparation for darkfield imaging:

Glass slides and coverslips were cleaned using Alconox® detergent, ethanol, and deionized water, respectively followed by drying in an oven. A 10 μL aliquot of Au-polyester NPs were diluted in 5 mL ethanol. The NPs were then drop-coated onto a cleaned glass slide and allowed to air dry. Finally, a drop of Cytoviva immersion oil was placed on the dried nanoparticles and covered with a coverslip. The seams between the coverslip and glass slide was sealed using a clear nail polish.

Hyperspectral imaging:

Gold nanoparticles were imaged using an enhanced dark field transmission optical microscope (Olympus BX41) equipped with a hyperspectral imaging spectrophotometer (CytoViva Hyperspectral Imaging System (HSI), Auburn, AL). The hyperspectral imager (mounted on a microscope and controlled by Environment for Visualization software (ENVI 4.4 version) from ITT Visual Solutions) extracted complete spectral information from single or multiple pixels. All images were taken using a 60X oil with iris objective at identical exposure time (0.6 ms). Nanoparticle intensity was calculated by averaging multiple pixels and normalized by dividing lamp spectral intensity.

3. Results and Discussion

3.1. One-step formulation of Au-PDLLA-PEG-COOH NPs

As described in the supporting information, a tin-mediated ring opening polymerization was used to synthesize PDLLA-PEG-COOH copolymer. The product was then purified, lyophilized, and characterized. The ^{1}H NMR spectrum revealed signals assigned to the expected copolymer (Figure S1). Next, we generated AuNPs within the PDLLA-PEG-COOH polymeric NPs using a photochemical reaction. To accomplish this task, we prepared PDLLA-PEG-COOH NPs with an encapsulated Au(III) salt and a photoinitiator

by means of a double emulsion/solvent evaporation methodology (Scheme 1). As detailed in the experimental section, organic and aqueous phases were mixed together by ultrasonic homogenization followed by addition of PVA surfactant. Additional homogenization produced a water/oil (W/O) microemulsion, which was then finally poured into a aqueous solution of PVA to create water-in-oil-in-water (W/O/W) nanoparticles after the removal of the organic solvent. The NPs were then washed and subsequently exposed to UV irradiation at 254 nm for 15–30 min. Purification and concentration of this isolate proceeded by means of filtration through centrifugal units or by dialysis to thoroughly remove any residuals in the solution. The irradiation protocol (254 nm) was conducted in the presence (*ex vivo*) and absence (*in vitro*) of chicken tissue in order to test the potential for on-demand and *in situ* preparation of the imaging agent. During UV exposure, gold NPs rapidly formed within the PDLLA-PEG-COOH NPs, resulting in the formation of a ruby/wine-colored solution in less than one min, indicative of the formation of AuNPs. The rapid formation of the AuNPs is due to the high local concentration of gold salt and initiator inside the PDLLA-PEG-COOH nanoparticle.

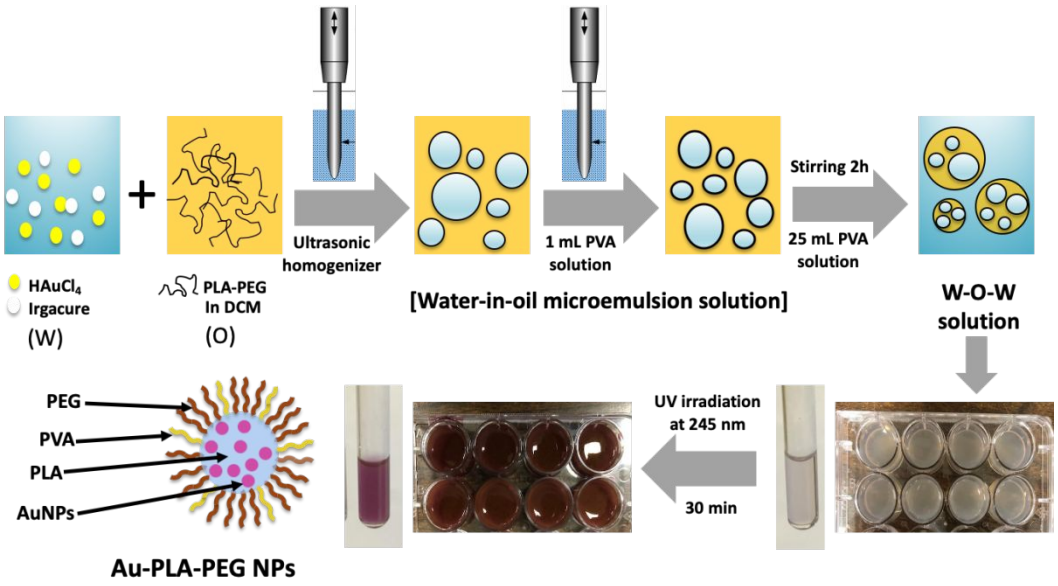

Scheme 1. Schematic representing the one-step synthesis of gold nanoparticles imbedded within PDLLA-PEG-COOH polymeric NPs. The protocol includes the introduction of the gold salt and photoinitiator into the polymeric NPs by the formation of a W/O/W emulsion, followed by solvent evaporation using an ultrasound generator, followed by exposure to UV irradiation (254 nm) for 30 min.

Specifically, the photochemical synthesis of AuNPs was promoted by the UV irradiation of encapsulated Irgacure photoinitiator (I-2959) and $HAuCl_4 \cdot xH_2O$. Irradiation with 254 nm light induces the formation of free radicals, which in turn reduce Au^{3+} to a combination of

Au^{2+} and Au^{0}, thus generating AuNPs as described elsewhere.[50] The efficiency of the photochemical process (Scheme S1) is such that upon exposure to 254 nm UV light, AuNP formation can be accomplished in a matter of minutes in sharp contrast to treatment of a solution of the Irgacure photoinitiator (I-2959) and $HAuCl_4 \cdot xH_2O$ without prior encapsulation in the polymeric NPs.

3.2. Characterization of the Au-PDLLA-PEG-COOH NPs

FTIR, ^{1}H NMR, TGA, DLS, TEM, XRD, and UV-vis spectroscopy techniques were used to characterize the physicochemical properties of the synthesized PDLLA-PEG-COOH and Au-PDLLA-PEG-COOH NP formulations. To confirm that the pre-encapsulation of the gold salt and photoinitiator was necessary for effective AuNP formation, we combined the gold salt and initiator in water in the absence of polymeric NPs. After UV treatment (15 min irradiation, 254 nm) we observed no detectable formation of AuNPs as confirmed by UV-vis spectroscopic analysis (Figure 1A). In contrast, the experiment with gold salt and initiator encapsulated in PDLLA-PEG-COOH NPs demonstrated clear evidence of AuNP formation (Figure 1B). These results suggest that the polymeric NPs serve to co-localize the Au(III) salt and the photoinitiator to promote an efficient reduction event leading to AuNP formation within the PDLLA-PEG nanoparticle. This reaction is evidently not possible in dilute solvent without the aid of polymeric NPs.

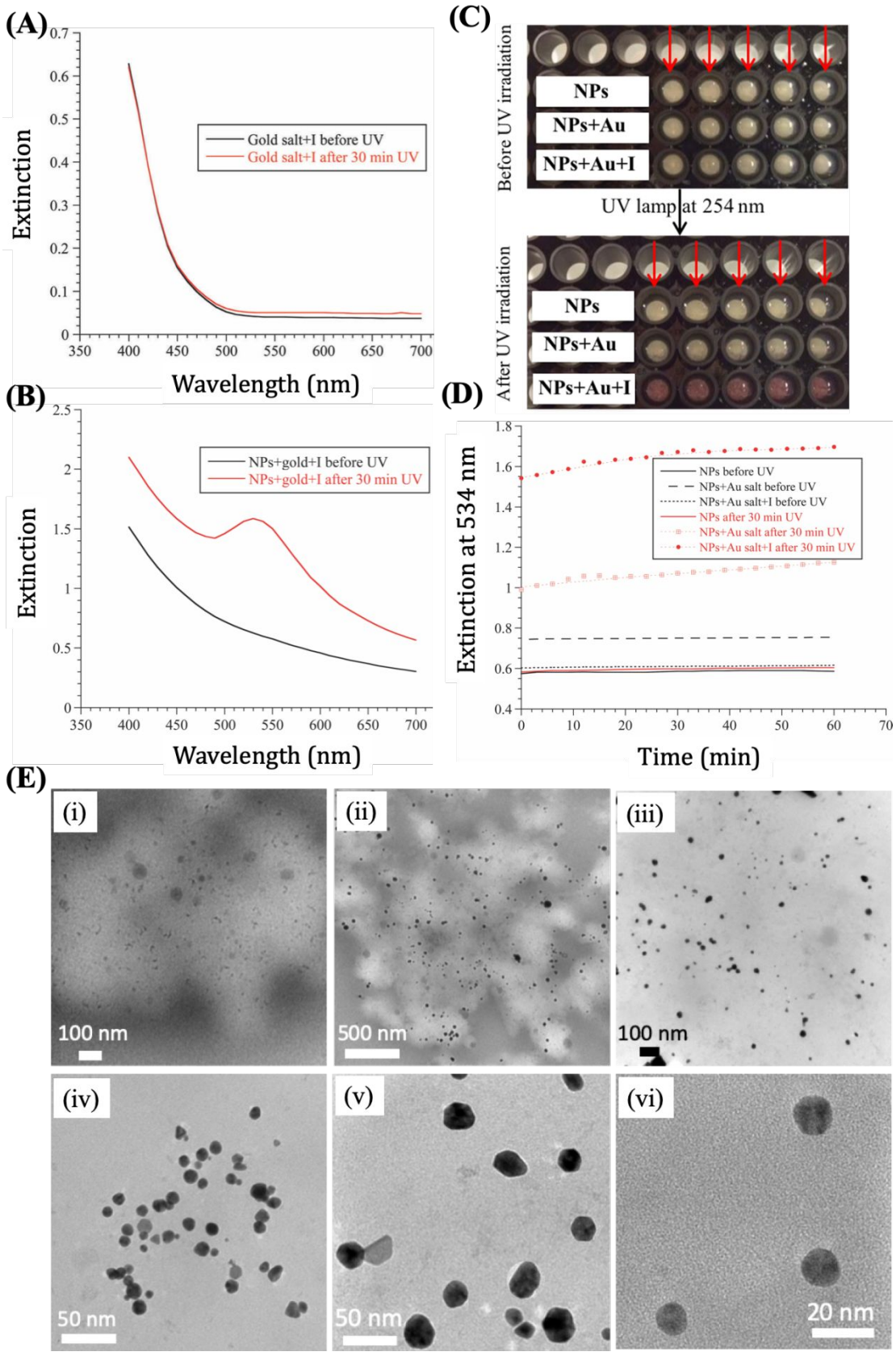

Figure 1. UV visible spectroscopic analysis of: **(A)** a solution of gold salt and initiator (*i.e.* not encapsulated in polymeric NPs) before (black line) and after (red line) 30 min UV irradiation; **(B)** a solution of gold salt and initiator encapsulated in PDLLA-PEG-COOH NPs before (black line) and after (red line) 30 min UV irradiation; **(C)** Digital photograph for two well-plates containing three kinds of nanoformulations before and after irradiation: i) PDLLA-PEG-COOH NPs, ii)

PDLLA-PEG-COOH NPs with gold(III) salt; and iii) PDLLA-PEG-COOH NPs incorporating gold(III) salt and initiator; **(D)** UV-vis kinetic measurements (534 nm) monitoring the nucleation and growth of AuNPs as a function of time. Three formulations of NPs (NPs alone, NPs+$HAuCl_4$, and NPs+ $HAuCl_4$+ I-2959) were tested before and after UV irradiation for 15 min. Each measurement was carried out five times (n=5). **(E)** Transmission electron microscopy (TEM) micrographs which demonstrate the fundamental difference in the contrast and the morphology between the PDLLA-PEG-COOH NPs alone (control) and the PDLLA-PEG-COOH NPs incorporating gold NPs: (i) PDLLA-PEG-COOH NPs, (ii-iv) gold-loaded PDLLA-PEG-COOH polymer NPs at different magnifications, and (v,vi) high resolution TEM for gold-loaded PDLLA-PEG-COOH polymer NPs.

To further emphasize the necessity of polymeric encapsulation of the reagents prior to AuNP synthesis, we prepared three formulations in parallel: PDLLA-PEG-COOH polymeric NPs, the polymeric NPs with encapsulated Au(III) salt, and polymeric NPs with encapsulated Au(III) salt and photoinitiator. Figure 1C shows that the characteristic ruby/wine color indicative of approximately spherical AuNP formation appeared after 30 min of UV irradiation only in the third row of the well-plate that contained both Au(III) salt and photoinitiator encapsulated in the polymeric nanoparticles. We further followed the nucleation and growth of the AuNPs kinetically by monitoring the UV-vis absorption at 534 nm over time (Figure 1D). This analysis revealed stable, flat absorbance traces before UV irradiation (*i.e.* no AuNPs generated) in all three formulations. After irradiation, no change occurred to samples containing PDLLA-PEG-COOH NPs lacking gold salt and initiator, while negligible changes were evident in the PDLLA-PEG-COOH NP sample containing Au(III) salt but lacking initiator.

TEM images of the materials were obtained immediately after formulation. Consistent with the DLS data (*vide infra*), the images indicate densely opaque, approximately spherical nanoparticles with a relatively homogeneous distribution within the sample. The measurements were done without the need for a staining agent. For comparison, we imaged the pure polymeric nanoparticles without gold (Figure 1E (i)) and found them to be significantly less contrasted as compared to the Au-PDLLA-PEG-COOH NPs (Figure 1E (ii-vi)). This discrepancy provides further evidence for the successful photochemical preparation of gold NPs within the polymeric NP matrix. Figure 1E (iv-vi) also highlight the mainly spherical shape and good homogeneity of the NPs.

Next, the growth of AuNPs as a function of irradiation time was monitored by recording the UV signal at ~534 nm – arising from the AuNP formation – before and after UV irradiation for 50 min. To investigate the effects of the concentration of all constituents on the growth of AuNPs, we conducted five parallel experiments in 1 mL final colloidal solution where

AuNPs were generated using increasing loadings of the polymeric NPs, Au(III) salt, and photoinitatior. Specifically, we probed the use of 0, 25, 50, 100, 200 mg of the polymer with variable loadings of Au(III) salt and photoinitiator as outlined in Table 1. The five samples were monitored by UV-vis spectroscopy before and after 50 min of UV irradiation to follow the nucleation and growth of AuNPs over time.

Table 1. Different concentrations of all ingredients to form 1 mL solutions of Au-PDLLA-PEG polymer NP suspension. Formulations 2-5 have increasing concentration of reagents, but constant relative concentrations.

#NPs	Polymer (mg)	Au(III) (mmol)	Irgacure (mmol)	Final NP solution (mL)
1	25	0	0	1
2	25	9.6	21.4	1
3	50	19.2	42.8	1
4	100	38.4	85.6	1
5	200	76.8	171.2	1

The spectra depicted in Figure 2A showed the gradual emergence of new peaks at 534 nm in the four formulations containing gold and initiator, indicating the formation of AuNPs after irradiation. A regular increase in the absorbance was recorded which has a direct correlation with the gold(III) concentration, while no absorbance peaks at 534 nm were evident in the case of the formulation lacking gold and initiator (*i.e.* NPs 1, Table 1).

Absorbance values of all samples were determined at different interval times (5 min rate) before and after UV exposure as indicated in Figure 2C and D. Since irradiation is necessary for AuNP generation, essentially no change in the UV spectrum was observed over time in the absence of light (Figure 2C). In contrast, a rapid emergence of a new absorbance band was apparent after 1 min of irradiation time in all four samples containing gold and photoinitiator reaching completion within 5, 7, and 15 min for the 25, 50, and 100 mg polymer formulations, respectively (Figure 2D). At the highest loading of polymer, gold, and photoinitiator (*i.e.* 200 mg polymer, 76.8 mmol Au^{3+}, 171.2 mmol photoinitator), we found that the nucleation and growth of AuNPs continues over the course of the entire 50 min irradiation period. These data clearly demonstrate the ability to formulate AuNPs within the polymeric NPs by means of a convenient photochemical reaction.

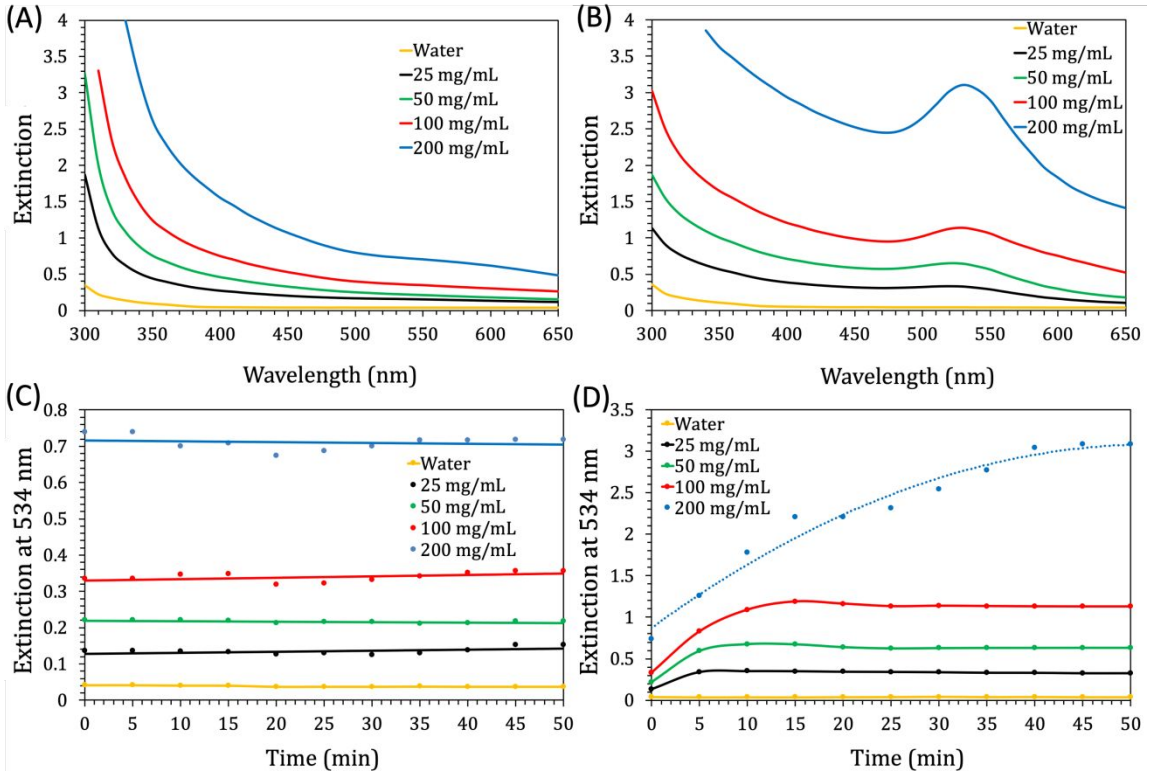

Figure 2. UV-vis spectroscopic analysis of the five nanoparticle formulations (see Table 1); (A and B) UV−vis absorbance spectra before and after 30 min UV irradiation, respectively. (C and D) plot of absorbance resulting from AuNP formation versus time, without irradiation (C) and with irradiation (534 nm) (D). Spectra were recorded at 5 min intervals.

In order to show the potential application for *in situ* generation of Au-polyester NPs, we explored their preparation by irradiation through a barrier of chicken muscle tissue (*ca.* 2 mm thickness). Thus, we positioned the UV lamp approximately 1 cm above the chicken tissue, which was used to cover a 96-well plate containing the reagents necessary for Au-polyester NP formation (Figure S2). UV-absorption spectroscopy, kinetic measurements and TEM analyses of the Au-polyester NPs generated in this experiment are shown in Figure 3. After a 30 min irradiation period, a weak band is observed at ~535 nm, superimposed on a background spectrum from scatter (Figure 3A). This 535 nm peak indicates the formation of a low concentration of AuNPs unlike the sharp band that appeared in the absence of chicken tissue (*cf.* Figure 2B). The growth of AuNPs was also monitored over the course of a 60 min irradiation period, showing a modest increase (see Figure 3B). The TEM images demonstrated the successful generation of the Au-polyester NPs in moderate concentration by means of UV-radiation through a tissue barrier (Figure 3C).

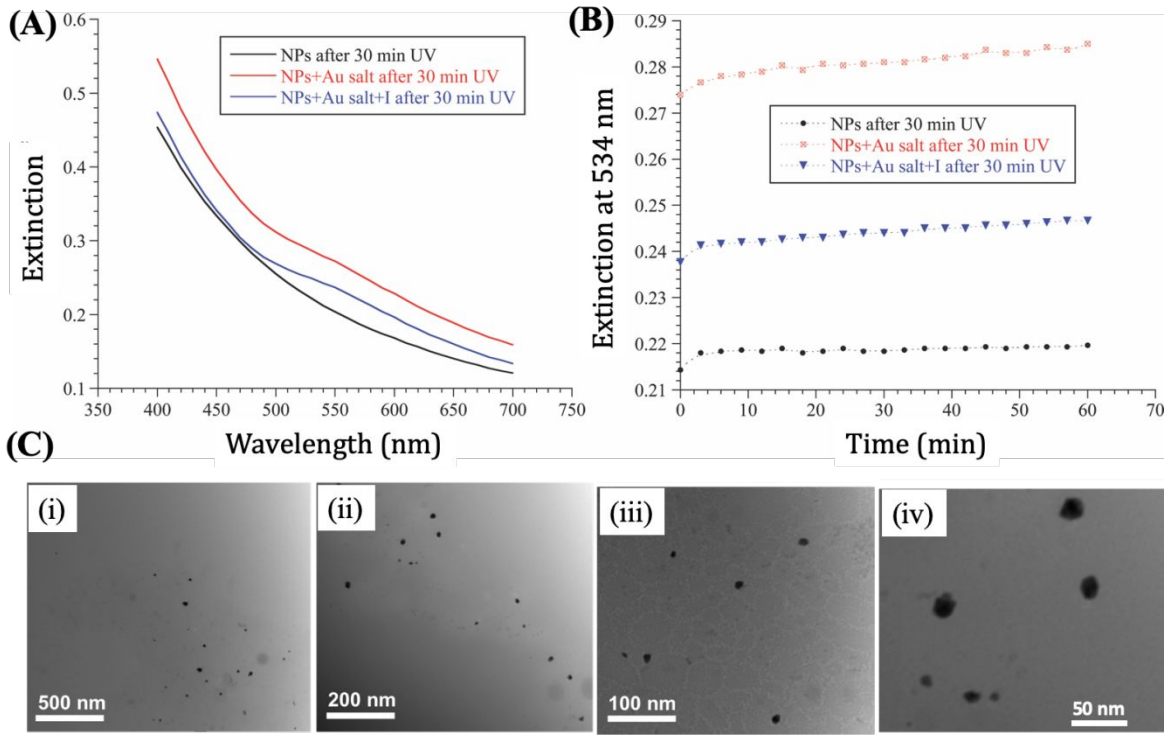

Figure 3. (A): UV absorbance spectra after 30 min UV irradiation of three polymeric NP formulations; NPs in water (control, black line), gold salt encapsulated within NPs (red line), and gold salt/photoinitiator encapsulated within polymer NPs (blue line). The experiments conducted by UV irradiation through a chicken muscle tissue (~ 2 mm thickness) barrier at 1 cm distance from the UV lamp. **(B):** Kinetic growth spectra (UV-vis) of Au-polymer NPs which shows a modest gradual nucleation of the gold NPs within the polymer NPs upon UV irradiation through tissue barrier. (C) TEM photographs for one sample of Au-polymer NPs with different scale bars (i.–iv.). These particles were generated by means of UV irradiation (254 nm; 30 min) through a chicken muscle tissue barrier. All spectral measurements were calculated as the average of quintuplicate runs.

Figure 4 outlines the X-ray diffraction (XRD) pattern of the polymeric NPs (control), Au-polymeric NPs, and Au-polymeric NPs generated by UV-irradiation through a tissue barrier (Figure S2). The XRD of the polymeric nanoparticles revealed the presence of a distinct peak at 2θ: 19.5˚ which is present in all three curves. Additional peaks corresponding to the presence of Au NPs were apparent at 2θ: 38.2˚, 44.4˚, and 64.6˚ in the sample prepared with and without irradiation through the tissue barrier, providing further evidence of the efficient formation of Au-polymeric NPs in both experiments.

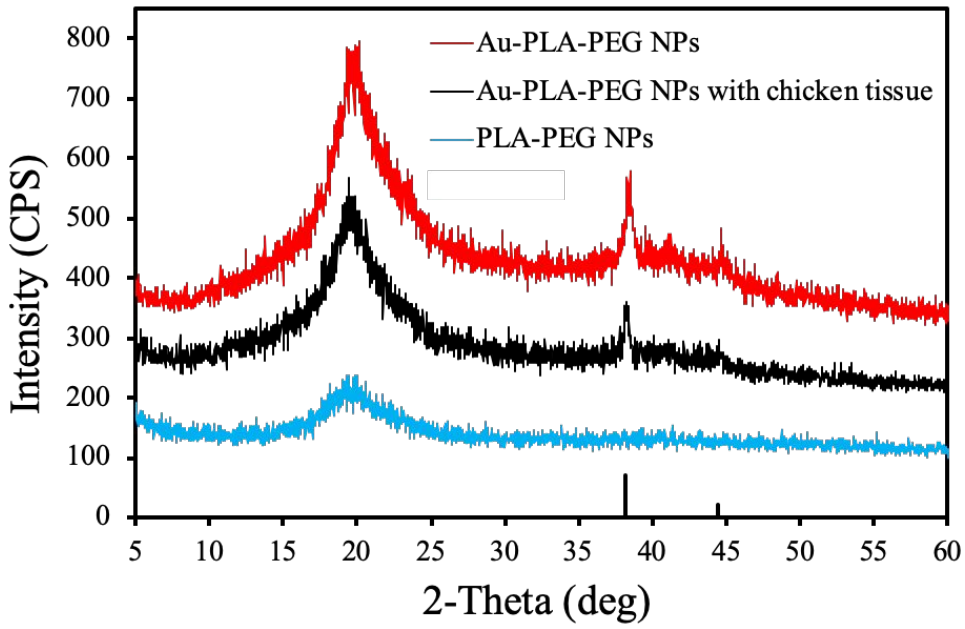

Figure 4. Powder X-ray diffraction (XRD) analyses of three nanoparticles formulations as indicated by colors.

Figure S3 depicts the overlaid infrared spectra of the pure PDLLA-PEG-COOH polymer NPs and Au-polyester NPs prepared in the presence and absence of the chicken muscle tissue barrier. These data indicate nearly identical IR spectra for the three formulations. Additionally, Figure S4 depicts TGA analyses of PDLLA-PEG-COOH polymer, PDLLA-PEG-COOH NPs, and Au-polyester NPs prepared in the presence and absence of the chicken muscle tissue barrier. The TGA analyses revealed significant changes in the thermal degradation of the bulk polymer as compared to the NP formulations. Nevertheless, the three polymeric formulations exhibited similar thermal degradation profiles.

Next, we studied the physical properties (*i.e.* size, surface charge, and polydispersity) of the resulting Au-polyester NPs resulting from different polymer and gold concentrations by means of DLS measurements (Figure 5). For this study, we characterized three nanoformulations (*i.e.*, NP1, NP2, and NP5; Table 1). They all provided narrow size distributions centered around 50, 106 and 60 nm, respectively (Figure 5A). All formulations were stable over a five week period after preparation confirming the excellent stability of the formulations upon prolonged storage at room temperature (Figure 5B and 5C). The particles remained monodisperse (PDI < 0.2) over the 5 week storage period (Figure 5C) and revealed a high negative charge – up to –37 mV – on their surface (Figure 5D). This highly negative surface charge likely arises from the surface carboxylates of the polyester NP.

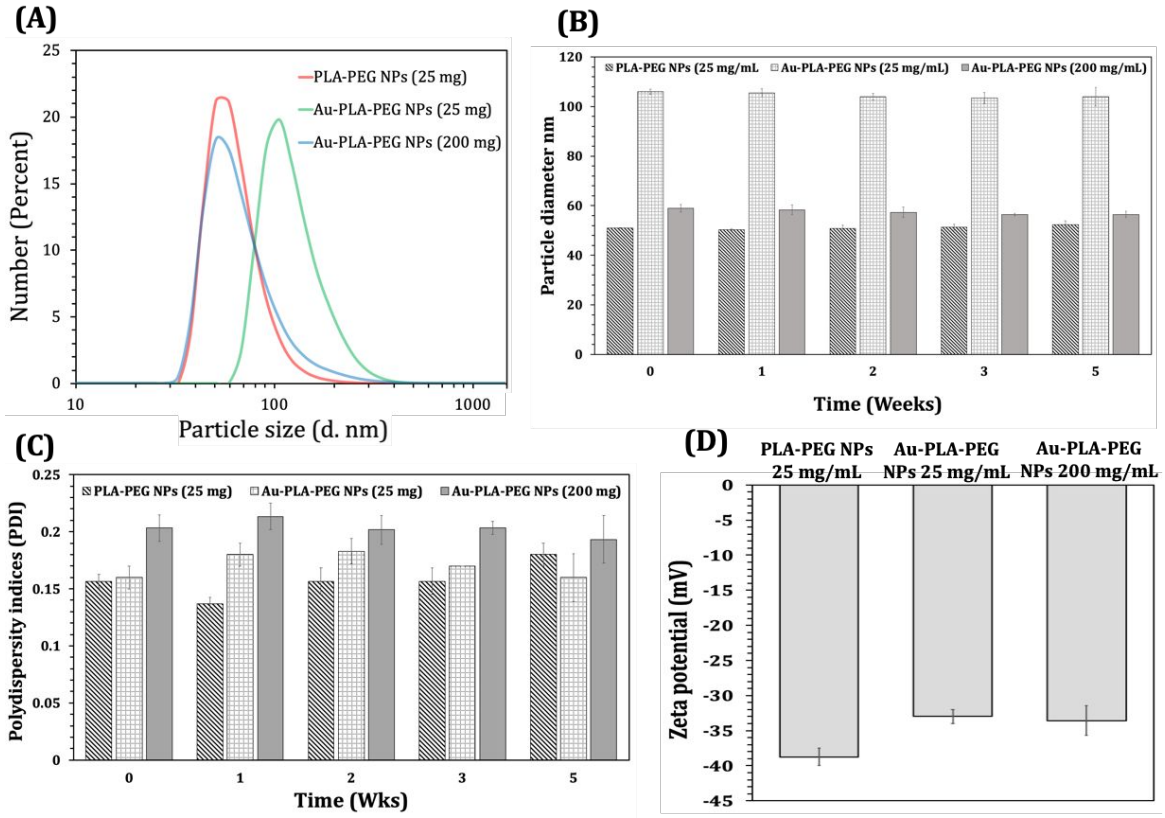

Figure 5. DLS measurements of three formulations; PDLLA-PEG-COOH NPs (25 mg), Au-polyester NPs (25 mg polymer loading), and Au-polyester NPs (200 mg polymer loading). (A) NP diameter, (B) Size stability over time up to 5 weeks, (C) PDI over time, and (D) zeta potential measurements representing a highly negative surface charge of all nanoformulations.

Additional *in vitro* studies were carried out on the synthesized nanoparticles to ensure their stability in blood serum. The three previous formulations with different concentrations of polymer (*i.e.*, NP1, NP2, and NP5; Table 1) were introduced into FBS by mixing 0.1 mL of each NP formulation with 0.9 mL FBS (10x dilution). The samples were then housed in an incubator at 37 ˚C under a controlled atmosphere (80% H_2O and 5% CO_2) for 24 h. The stability of the NP formulations was probed by monitoring the size of the NPs by means of DLS analysis versus time over a 24 h period (Figure 6 (top)). The results indicate no discernable change in the size for all three nanoformulations, meaning that the NPs are quite stable in blood.

Cytotoxicity assays were also performed with the same three formulations on 3T3 normal fibroblast cells to assess the possibility of adverse effects on cells (Figure 6 (bottom)). After one day incubation, we observed no discernible cytotoxicity of either the polymeric NPs (control) or the gold-polymer NPs formed *ex vivo* (*i.e.* prepared by irradiation through a chicken tissue barrier), while a very modest cell death was apparent upon dosing higher concentrations of Au-polyester NPs prepared by direct UV irradiation. The modest

cytotoxicity of the formulation prepared by direct UV irradiation (*i.e.* without a tissue barrier) is likely due to a higher density of Au-polyester NPs being generated in the sample. Overall the three formulations showed very low cytotoxicity in doses up to 500 μg NPs/mL on 3T3 fibroblast cells. In parallel, the same Au-polyester NP formulations were tested also on human glioblastoma U-87 MG cells and no cell death was found up to 500 μg/mL concentrations (Figure S5). These results provide strong evidence that the Au-polyester nanoparticles do not exhibit appreciable cytotoxicity, even at higher concentrations.

Next, we set out to evaluate whether the Au-polyester NPs could be formulated in the presecence of living cells in culture medium. We cultured adipose stromal cells (ASC) and then added pre-synthesized PLA-PEG-COOH NPs containing gold salt and the photoinitiator. We next exposed the cells and NPs to UV irradiation for 30 min to generate the Au-polyester NPs. We observed the formation of Au-polyester NPs visually by the appearance of a pink color in the culture medium, which was confirmed by UV spectral analysis, revealing the characteristic absorbance peak at a wavelength of 535 nm. In order to assess the cytotoxicity of the formulation protocol we generated two control cultures for comparison: ASCs exposed to 30 min UV irradiation and ASCs that were protected from UV irradiation. We compared these control samples against four trials of our UV irradiation protocol that resulted in increasing concentrations of Au-polyester NPs: 390.5, 781, 1526, and 3125 μg/mL. Figure S6 indicates nearly identical levels of cell viability as compared to the two controls for the 390.5 μg/mL, which confirms the successful synthesis of the Au-polyester NPs in the presence of living cells. In contrast, cell viability was reduced in the prescence of higher concentrations of Au-polyester NPs.

Thus, we believe that these materials may prove useful for studying cellular functions/mechanisms in culture without impacting cell viability. Our results are consistent with a study reported by Buonanno *et al.* that demonstrated that 254 nm UV irradiation, while having serious safety considerations, did not produce UV-associated DNA lesions in a 3D skin model and exhibited low cytotoxicity to exposed mammalian skin.[51] Moreover, it is expected that the length of exposure and repeated exposure could increase the risk, but our proposed method only requires one short exposure.

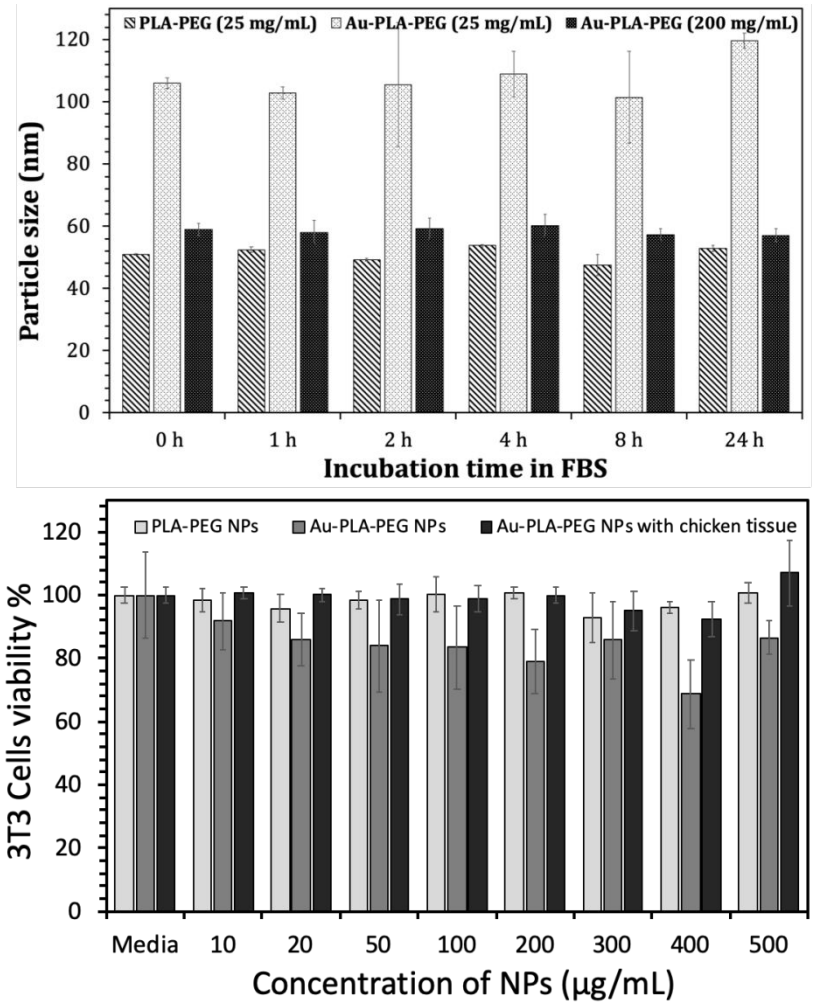

Figure 6. *In vitro* studies; (top) Size stability of the NP formulations in fetal bovine serum over 24 h. (bottom) One day-3T3 fibroblast cell viability at different concentrations of Au-polyester NPs generated by irradiation with or without a tissue barrier, along with the control polymeric NPs. Results as presented as means ± standard deviation. All the experimental studies were performed in sextuplicate.

3.3. Plasmonic surface resonance

Gold nanoparticles have interesting optical properties depending on their size, their shape, and the refractive index of the surrounding medium. When the Au-polyester NPs were illuminated with white light, they appeared as green color points in darkfield microscopy images. Additionally, a few of the nanoparticles appeared red in color (Figure 7, left). This discrepancy is likely due to aggregation of the Au-polyester NPs during sample preparation for SPR analysis (*i.e.* drop coating).

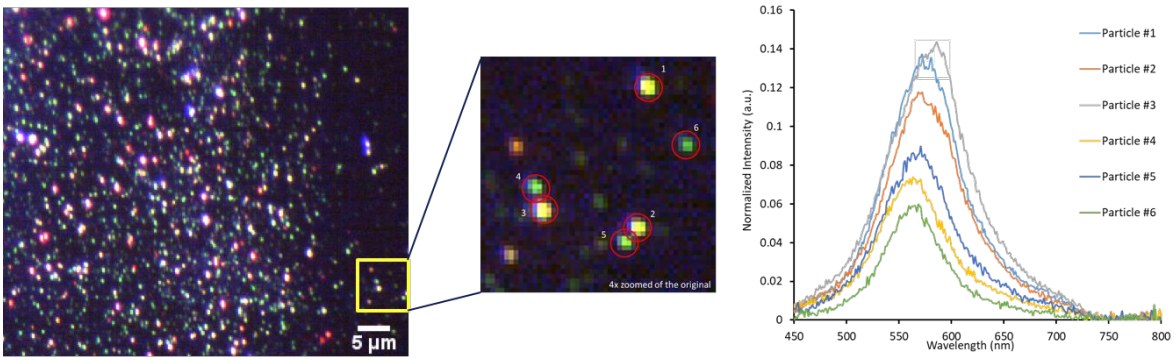

Figure 7: (Left) darkfield microscopy image representing the SPR properties of Au-polyester NPs. (Middle) darkfield microscopy image (4x magnification) representing individual nanoparticles corresponding to the presented scattering spectra. (Right) scattering spectra (normalized to the lamp spectrum) corresponding to the encircled nanoparticles (see inset image at left).

Single Au-polyester nanoparticles were clearly observed in the dark-field image (and more clearly in the magnified inset) (Figure 7). Single-particle scattering spectra corresponding to the resulting nanoparticles are shown in Figure 7, at right. The average LSPR peak of Au-polyester NPs is *ca.* 569 nm. The slight shift in the LSPR peak is due to different sizes and shapes of the NPs and the refractive index of the Cytoviva immersion oil used for the experiment. These results validate the excellent plasmonic properties of the Au-polyester NPs.

3.4. Cellular uptake and endosome-entrapment of Au-polyester NPs

Raw murine cells (normal cell model) and U-87 MG glioblastoma cells (cancer cell model) were prepared and incubated in the presence of two concentrations of Au-polyester NPs (500 and 1000 µg/mL) for 1 h and 24 h. The cell samples were then washed three times with phosphate-buffered saline (PBS) to remove free particles from the cell medium before imaging. The confocal settings were performed as it was described by Kim *et al*.[49] The Au-polyester NPs were clearly visualized inside the two cell lines due to a high degree of internalization. As can be seen in Figure S7, scattering signals were very low at 1 h incubation time in both cell lines at high concentration of the NPs (1000 µg/mL). Higher signals (marked in red) were detected after significant internalization by the cells over the 24 h incubation time at the same concentration as shown in Figure 8.

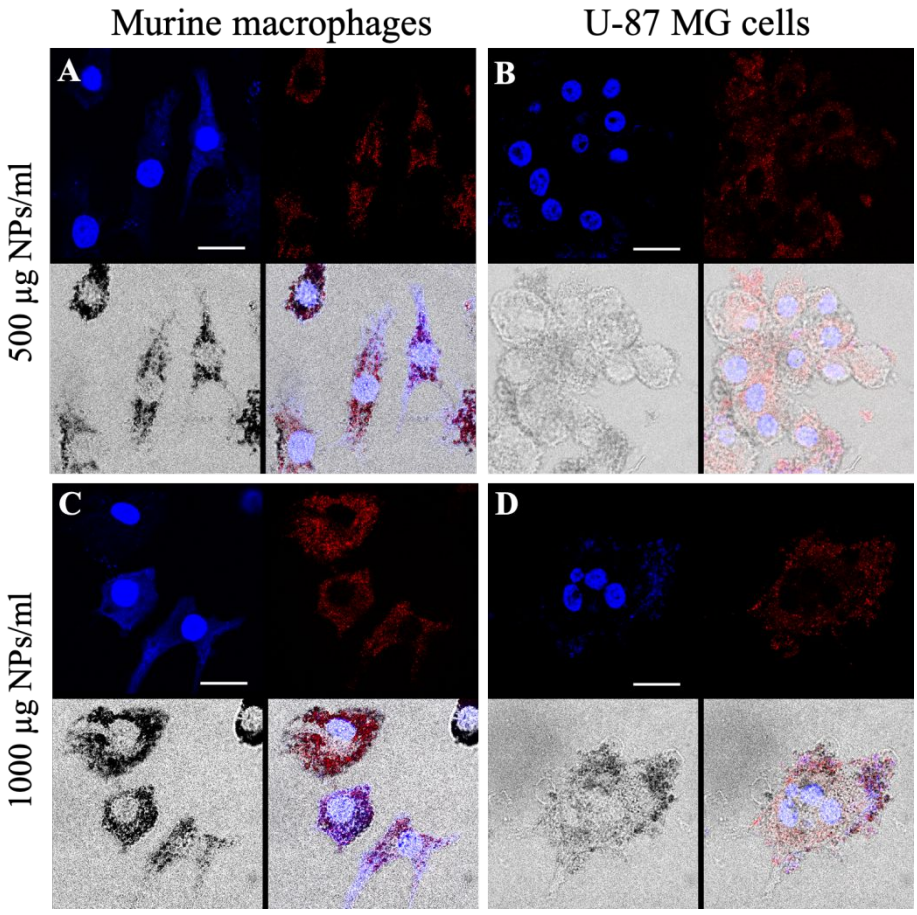

Figure 8. Cellular uptake images of the synthesized Au-polyester NPs *in vitro*. Typical images (glioblastoma and RAW 264.7 cells, 24 h incubation, 500 and 1000 µg/mL indicated in the 4 channels) (A-D). Each channel contains blue color which indicates nuclei and particularly, cytoplasm (upper-left corner), red color indicates presence of Au-polyester NPs (upper-right corner), white-black image is the DIC image of the cells (lower left corner), and overlay (lower right corner). Scale-bar is 20 µm.

We noticed a comparable uptake of the Au-polyester NPs in both cell lines after a short, one-hour incubation time. After 24 h of incubation, the entire cytoplasm is filled with red NPs in both cell lines. Nonetheless, a bit higher uptake was observed in macrophages as compared to glioblastoma cells after 24 h due to phagocytosis. These images demonstrate that the Au-polyester NPs were entirely localized in the late endosome/lysosome after 24 h, and the observed scattering imaging intensity is time dependent. These observations are similar to what was described previously, demonstrating the capability of Au-polyester NPs to be efficiently internalized into cells.[52] These *in vitro* experiments were designed as a preamble for *in vivo* examination in the future. We hypothesize that the PDLLA-PEG-COOH NPs containing the gold salt and photoinitiator will circulate in the blood, accumulate in tissues, and then remain in a localized region due to their facile internalization into cells. Then, the Au-polyester NPs can be prepared in situ by exposure to

UV irradiation. The concentration of the gold salt and photoinitiator is critical, and can be effectively controlled by encapsulating the materials into the PDLLA-PEG-COOH NPs.

4. Conclusions

As opposed to the common methodologies reported in the literature for the synthesis of AuNPs loaded in polymeric NPs, herein we synthesized polymer NPs containing a gold(III) salt and photoinitiator that are efficiently transformed into Au-polyester NPs on demand by means of a convenient photochemical reaction within the polymer NP formulation. Uniform spherical Au-polyester NPs with high negative surface charge of –37 mV and a controlled size (*i.e.*, 50 and 106 nm) were obtained according to variations in the concentrations of the polymer, Au(III) salt, and initiator prior to irradiation. The Au-polyester NPs can be generated by irradiation through a tissue barrier, indicating the potential for this strategy to be used *in vivo*. Toward this end, the formulation developed herein exhibited very high stability in blood serum and negligible *in vitro* cytotoxicity against 3T3 fibroblast and glioblastoma cell lines. The photothermal synthesis of the Au-polyester NPs can be effected in the presence of living cells without causing appreciable cytotoxicity, despite the use of UV irradiation. The Au-polyester NPs also exhibited outstanding SPR and cellular imaging properties. The significance of this contribution arises from the ability to prepare an appropriate imaging agent *in situ* by means of a convenient photochemical process in lieu of more conventional *ex situ* approaches. Current efforts in our group are centered on improving the efficiency of this protocol and testing the Au-polyester NPs using relevant animal models.

Conflict of interest

The authors have no conflicts to declare.

Acknowledgements

We thank the Clemson Light Imaging Facility (CLIF) which is supported, in part, by the Clemson University Division of Research, NIH EPIC COBRE Award #P20GM109094, and NIH SCBiocraft COBRE Award #5P20RR021949-03. The CytoViva hyperspectral microscope purchase was also supported in part with funds from NSF MRI Award #1126407. We also acknowledge the Ministry of Education and Science of the Russian Federation in the framework of Increase Competitiveness Program of NUST «MISiS» (№ К4-2018-052), implemented by a governmental decree dated 16th of March 2013, N 211.

We thank Ms. Cassie George for assistance with some aspects of the cellular work described herein.

References

1 P. Suchomel, L. Kvitek, R. Prucek, A. Panacek, A. Halder, S. Vajda and R. Zboril, *Sci. Rep.*, 2018, **8**, 1–11.
2 D. Huang, F. Liao, S. Molesa and D. Redinger, *J. Electrochem. Soc.*, 2003, **150**, 412–417.
3 T. Minari, Y. Kanehara, C. Liu, K. Sakamoto and T. Yasuda, *Funct. Mater.*, 2014, **24**, 4886–4892.
4 Y. Su, Y. Ke, S. Cai and Q. Yao, *Light-Sci. Appl.* 2012, **1**, 2–6.
5 M. Notarianni, K. Vernon, A. Chou, M. Aljada, J. Liu and N. Motta, *Sol. Energy*, 2014, **106**, 23–37.
6 K. Sokolov, M. Follen, J. Aaron, I. Pavlova, A. Malpica, R. Lotan and R. Richards-kortum, *Cancer Res.*, 2004, **9** 1999–2004.
7 X. Huang and M. A. El-sayed, *Adv. Res.*, 2010, **1**, 13–28.
8 D. P. O. Neal, L. R. Hirsch, N. J. Halas, J. D. Payne and J. L. West, *Cancer Lett.*, 2004, **209**, 171–176.
9 L. C. Kennedy, L. R. Bickford, N. A. Lewinski, A. J. Coughlin, Y. Hu, E. S. Day, J. L. West and R. A. Drezek, *Small*, 2011, **2**, 169–183.
10 C. Loo, L. Hirsch, M. Lee, E. Chang, J. West, N. Halas and R. Drezek, *Opt. Lett.,* 2005, **30**, 1012–1014.
11 P. A. Thompson, Æ. S. M. Blaney and J. L. West, *J. Neurooncol.*, 2008, **86**, 165–172.
12 A. J. Coughlin, J. S. Ananta, N. Deng, I. V Larina, P. Decuzzi and J. L. West, *Small*, 2014, **3**, 556–565.
13 A. M. Gobin, E. M. Watkins, E. Quevedo, V. L. Colvin and L. West, *Small*, 2010, **6**, 745–752.
14 P. Singh, S. Pandit, V. R. S. S. Mokkapati, A. Garg, V. Ravikumar and I. Mijakovic, , *J. Mol. Sci.* 2018, **19,** 1979–2004.
15 N. S. Abadeer and C. J. Murphy, *J. Phys. Chem. C*, 2016, **120**, 29423-29431.
16 D. Medhat, J. Hussein, M. E. El-Naggar, M. F. Attia, M. Anwar, Y. A. Latif, H. F. Booles, S. Morsy, A. R. Farrag, W. K. B. Khalil and Z. El-Khayat, *Biomed. Pharmacother.*, 2017, **91**, 1006–1016.
17 R. S. Riley and E. S. Day, *Wiley Interdiscip. Rev.-Nanomed. Nanobiotechnol.*, 2017, **9**, 1–16.
18 E. C. Dreaden, L. A. Austin, M. A. Mackey, M. A. El-Sayed, *Ther. Deliv.*, 2013, **3**, 457–478.
19 J. Liu, M. Yu, C. Zhou, S. Yang, X. Ning and J. Zheng, *J. Am. Chem. Soc.*, 2013, **135,** 4978–4981.
20 J. D. Mangadlao, X. Wang, C. Mccleese, M. Escamilla, G. Ramamurthy, Z. Wang, M. Govande, J. P. Basilion and C. Burda, *ACS Nano*, 2018, **12**, 3714–3725.
21 B. Duncan, C. Kim and V. M. Rotello, *J. Control. Release*, 2010, **148**, 122–127.
22 D. Pissuwan, T. Niidome and M. B. Cortie, *J. Control. Release*, 2011, **149**, 65–71.
23 M. M. Mahan and A. L. Doiron, *J. Nanomater.*, 2018, **2018**, 1–25.
24 M. F. Attia, J. Wallyn, N. Anton and T. F. Vandamme, *Crit. Rev. Ther. Drug Carrier Syst.*, 2018, **35**, 391–431.

25 Z. Wu and W. Wu, *Nanoscale*, 2016, **8**, 1237–1259.
26 H. Y. Son, K. R. Kim, C. A. Hong and Y. S. Nam, *ACS Omega*, 2018, **3**, 6683–6691.
27 Y. Chen, Y. Xianyu and X. Jiang, *Acc. Chem. Res.*, 2017, **50**, 310–319.
28 P. Zhao, N. Li and D. Astruc, *Coord. Chem. Rev.*, 2013, **257**, 638–665.
29 S. Gomez, K. Philippot and V. Colli, *Chem. Commun.*, 2000, **12**, 1945–1946.
30 X. Liu, M. Atwater, J. Wang, Q. Dai, J. Zou, J. P. Brennan and Q. Huo, *J. Nanosci. Nanotechnol.*, 2007, **7**, 3126–3133.
31 M. Brust, M. Walker, D. Bethell, D. J. Schiffrin and R. Whyman, *J. Chem. Soc., Chem. Commun.,* 2000, **7**, 801–802.
32 Y. Jin, P. Wang, D. Yin, J. Liu, L. Qin, N. Yu, G. Xie and B. Li, *Colloid Surf. A-Physicochem. Eng. Asp.*, 2007, **302**, 366–370.
33 M. Vinod, R. S. Jayasree and K. G. Gopchandran, *Curr. Appl. Phys.*, 2017, **17**, 1430–1438.
34 E. Giorgetti, A. Giusti, S. C. Laza, P. Marsili and F. Giammanco, *Phys. Status Solidi A-Appl. Mat.*, 2007, **204**, 1693–1698.
35 M. Yamamoto, Y. Kashiwagi and M. Nakamoto, *Z. Naturforsch.*, 2009, **64**, 1100–1305.
36 G. Cardone, G. Carotenuto, A. Longo, P. Perlo and L. Ambrosio, *EXPRESS Polym. Lett.*, 2007, **1**, 604–607.
37 S. Dong and S. Zhou, *Sci. Eng. B,* 2007, **140**, 153–159.
38 F. Kim, J. H. Song and P. Yang, *J. Am. Chem. Soc.,* 2002, **124**, 14316–14317.
39 K. Mallik, M. Mandal, N. Pradhan and T. Pal, *Nano Lett.*, 2001,**6**, 1–4.
40 A. Pal, S. K. Ghosh, K. Esumi and T. Pal, *Langmuir*, 2004, **20**, 575–578.
41 W. C. Vries, M. Niehues, M. Wissing, T. Würthwein, F. Mäsing, C. Fallnich, A. Studer and B. J. Ravoo, *Nanoscale*, 2019, **11**, 9384–9391.
42 N. T. K. Thanh, N. Maclean and S. Mahiddine, *Chem. Rev.*, 2014, **114**, 7610-7630.
43 M. J. Cheng, P. Prabakaran, R. Kumar, S. Sridhar and E. E. Ebong, *J. Vis. Exp.*, 2018, **131**, 56760–56744.
44 H. Ferreira, A. Martins, L. Alves, S. Amorim, S. Faria, R. A. Pires, R. L. Reis and N. M. Neves, *J. Mater. Chem. B*, 2018, **6**, 16–18.
45 E. Boisselier, A. K. Diallo, L. Salmon and J. Ruiz, *J. Am. Chem. Soc.*, 2010, **132**, 2729–2742.
46 M. K. Corbierre, N. S. Cameron, M. Sutton, S. G. J. Mochrie, L. B. Lurio and A. Ru, *J. Am. Chem. Soc.*, 2001, **123**, 10411–10412.
47 M. J. Ramalho and M. C. Pereira, *J. Chem. Educ.*, 2016, **93**, 1446-1451.
48 G. Road and E. B. Park, *J. Aerosol Sci.*, 2010, **30**, 4439–4451.
49 C. S. Kim, X. Li, Y. Jiang, B. Yan, M. Ray, D. J. Sol and V. M. Rotello, *MethodsX*, 2015, **2**, 306–315.
50 M. L. Marin, K. L. Mcgilvray and J. C. Scaiano, *J. Am. Chem. Soc.,* 2008, **130**, 16572–16584.
51 M. Buonanno, B. Ponnaiya, D. Welch, M. Stanislauskas, G. Randers-Pehrsona, L. Smilenov, F. D. Lowy, D. M. Owens and D. J. Brenner, *Radiat. Res.*, 2017, **187**, 483–491.
52 A. B. Witte, A. N. Leistra, P. T. Wong, S. Bharathi, K. Re, P. Smith, O. Kaso, K. Sinniah and S. K. Choi, *J. Phys. Chem. B* 2014, **118**, 2872−2882.

In Situ Preparation of Gold-Polyester Nanoparticles for Biomedical Imaging

Mohamed F. Attia,[a] Meenakshi Ranasinghe,[a] Roman Akasov,[c,d] Jeffrey N. Anker, [a] Daniel C. Whitehead, [a] and Frank Alexis[b*]*

[a]Department of Chemistry, Clemson University, Clemson, SC, USA
[b]School of Biological Sciences and Engineering, Yachay Tech, San Miguel de Urcuquí, Ecuador
[c]National University of Science and Technology «MISIS», Leninskiy Prospect 4, 119991 Moscow, Russia
[d]I.M. Sechenov First Moscow State Medical University, 119991, Trubetskaya str. 8-2, Moscow, Russia

Submitted to: ***Biomaterials Science***

Corresponding Authors: Frank Alexis (falexis@yachaytech.edu.ec) and Daniel C. Whitehead (dwhiteh@clemson.edu)

Graphical abstract: